DOI: 10.1002/((please add manuscript number))
Article type: Research Articles

Rapid Lithium Diffusion in Order@Disorder Pathways for Fast-Charging Graphite Anodes

*Wenlong Cai, Chong Yan, Yu-Xing Yao, Lei Xu, Rui Xu, Li-Li Jiang, Jia-Qi Huang, and Qiang Zhang**

Dr. W. L. Cai, Y.-X. Yao, Dr. L. L. Jiang, Prof. Q. Zhang,
Beijing Key Laboratory of Green Chemical Reaction Engineering and Technology, Department of Chemical Engineering
Tsinghua University
Beijing 100084, China
E-mail: zhang-qiang@mails.tsinghua.edu.cn
C. Yan, L. Xu, R. Xu, Prof. J.-Q. Huang,
Advanced Research Institute of Multidisciplinary Science
Beijing Institute of Technology
Beijing 100081, China
Dr. L.L. Jiang
Key Laboratory for Special Functional Materials in Jilin Provincial Universities,
Jilin Institute of Chemical Technology
Jilin, 132022, China

Keywords: fast charging, graphite anode, porous carbon layer, lithium ion diffusion, three-electrode measurement

Abstract: The employment of graphite anode renders practical lithium ion batteries for effective energy storage. However, graphite anode is the bottleneck to achieve the fast-charging of a battery ascribing to its low operating potential and corresponding incidental lithium plating. Herein the principle of a thin nanoscale layer on graphite surface to improve charging capability is investigated by applying a three-electrode device to precisely record the working behavior. The Li^+ diffusion rate is significantly improved by coating a nanoscale turbostratic carbon layer, in which abundant active sites and additional fast Li^+ diffusion pathways at the basal-plane side of graphite sheets render small polarization in a working battery. This fresh understanding enriches the fundamental insights into enhancing the rate performance and facilitating the practical applications of graphite in fast-charging batteries.

1. Introduction

The exploration of energy chemistry in a working battery based on high-energy cathodes, robust electrolytes, and adaptable charging-discharging protocols makes lithium ion batteries (LIBs) as the most important energy storage systems for our current life.[1, 2] Owing to excellent reversibility of the Li^+ intercalation/de-intercalation, high Li^+ storage capacity (372 mAh g^{-1}), and abundant sustainable precursors, graphite anode is the most promising candidate for practical LIBs.[3] However, graphite anode is widely regarded as the main obstacle impeding the application of LIBs at high charging rates, which is attributed to its low operating potential and slow kinetics of Li^+ intercalation. Moreover, lithium plating on the surface of graphite is a potential risk that may subsequently cause performance deterioration or thermal runaway of LIBs.[4, 5]

Tremendous strategies have been devoted to improve the charging capability of graphite anodes at high rates.[4, 6, 7, 8] Regulating Li^+ solvation structure,[8] introducing artificial coating layer on graphite surface,[6, 9] modifying graphite bulk materials,[6, 10] and optimizing charging protocols,[2] are strongly considered recently. Particularly, precoating the surface of graphite particles with a thin polymers[11], inorganic compounds,[6, 9, 12, 13] and hybrid organic/inorganic layer is explored,[14] which can effectively inhibit the decomposition of electrolyte, increase initial Coulombic efficiency and reduce irreversible capacity loss. Most attentions are drawn on the characterization of the coating layers and the improved electrochemical performance of the graphite electrodes.[15] However, the in-depth mechanism of core-shell graphite anode for promoting fast-charging is the core energy chemistry topic for fully rechargeable cells with high-rate performance, which has not been deeply understood. Moreover, precisely purifying the electrochemical behaviors of graphite electrode without the complication of counter electrode is still a universal challenge in routine two-electrode batteries set-ups.[13, 16]

In this contribution, nanoscale turbostratic carbon coated graphite was chosen as a model system to probe the energy chemistry of fast charging. The 6.5 nm thick carbon coating layer

considerably improves initial Coulombic efficiency, specific capacity, and rate performance of graphite anode in a working battery. The three-electrode system was carried out to record the true behavior of working electrodes. It reveals that the turbostratic carbon coating layer on graphite surface possesses larger interlamellar spacing. This can provide more active sites for Li^+ intercalation and offer fast Li^+ transport due to its isotropy, resulting in reduced polarization and enhanced Li^+ diffusion, which are beneficial to improve the rate performance of graphite anode.

2. Results and dicusssion

The morphology of raw graphite (G) and turbostratic carbon coated graphite (G@TC) were compared and exhibited in **Figure 1 and S1**. The shape of both G and G@TC are flakes, with almost the same size of 10~50 μm (**Figure S1**). **Figure 1a** demonstrates only one kind of lattice fringe with 0.336 nm belonging to G, while for G@TC there is a uniform 6.5 nm thick turbostractic carbon layer coated on graphite, exhibiting a wavy-structure with a lattice spacing of 0.375 nm (**Figure 1b**). The Raman spectrum of G@TC depicts obvious disordered peak (1340 cm^{-1}) compared with G (**Figure S2a**), demonstrating a high degree of disorder of the carbon coating layer.[17] The specific surface area of G@TC is about 1.7 $m^2\ g^{-1}$ (**Figure S2b**), which is smaller than that of G (2.2 $m^2\ g^{-1}$), ascribing to the coverage of defects and pores of graphite sheets (**Figure S1**).[18] Besides, X-ray powder diffraction (XRD) patterns of G and G@TC particles exhibit almost identical characteristic diffraction peaks of graphite (PDF#26-1076), and the location of (002) peak are the same but become narrow (**Figure S3**). Furtherly, X-ray photoelectric spectroscopy (XPS) reveal that both G and G@TC show the same XPS survey spectra, and the O1s spectra display the same peaks, suggesting no other foreign elements were introduced into G material (**Figure S4**). In addition, it should be noted that the electrical conductivity of G@TC (28.6 S cm^{-1}) is comparable to that of G (34.4 S cm^{-1}), which measured by four point probe method.

The electrochemical performance of G and G@TC electrodes were explored and compared in routine two-electrode batteries. As shown in **Figure S5**, cyclic voltammetry (CV) was firstly

applied to investigate the electrochemical behavior, which exhibits typical redox peaks at a scanning rate of 0.1 mV s^{-1}. There is obvious reduction reaction between 0.2–0.6 V for G electrode. This is ascribed to large specific surface area of G and decomposition of electrolyte in these exposed defects or pore structure.[18] Meanwhile, the initial discharge curve of G electrode also exhibits a smaller slope during 0.2–0.6 V and consequently results in low initial Coulombic efficiency (**Figure S6**).

To evaluate the electrochemical cycling performance, rate capability and typical galvanostatic discharge/charge tests were performed. As depicted in **Figure 2a**, the capacity rises slightly at 0.2 C by coating G with a thin amorphous carbon layer. As current gradually increases, the capacity discrepancy becomes conspicuous, while the capacity of G@TC electrode is nearly twice that of G electrode at 3 C (**Figure 2b**), indicating the sufficient supply of Li^+ in the rate-determining step of intercalation. The long-term cycling performance of G@TC electrode is also superior than that of G electrode (**Figure S7**).

Besides, lithium plating, which is deemed thermodynamically favorable on graphite surface as the potential falls below 0 V,[19] is significantly delayed in the case of G@TC electrode at freezing 0°C comparing to that of G electrode (**Figure 2c and 2d**). Moreover, when coupling practical $LiFePO_4$ cathode with G@TC anode, it can achieve 87% capacity retention even after 300 cycles at 170 mA g^{-1}, which is superior than that of with G anode (70% capacity retention after 250 cycles) (**Figure S8**). Therefore, the coating of nanoscale turbostratic carbon layer benefits electrochemical performance of graphite electrode, especially at high rates (such as 2 and 3 C), indicating the rapid transportation of Li^+. These results motivate us to further explore the in-depth mechanism of the improved Li^+ diffusion rate in G@TC anode.

XPS was applied to identify the difference of solid electrolyte interphase (SEI) of G and G@TC electrodes (**Figure S9**). The XPS survey spectra reveal roughly the same peaks, suggesting identical elements present on the surface of both G and G@TC. The F 1s spectra, Li 1s spectra, and C 1s

spectra all exhibit the same kind of substance belonging to LiF, Li_2O, Li_2CO_3, Li_xPF_y, $Li_xPO_yF_z$, and $ROCO_2Li$, etc.,[20] while the only difference is that the higher proportion C-C bond at 284.8 eV on G@TC surface attributing to the turbostratic carbon coating layer. In addition, differential scanning calorimetry (DSC) experiments further depict the same SEI decomposition peak (**Figure S10**).[21] Therefore, there is negligible difference on the components of SEI between G and G@TC, indicating the altering of SEI chemistry should not be the major attribution for the performance enhancement after coating the turbostratic carbon layer.

A three-electrode device was then applied to precisely record the status energy barrier of Li^+ diffusion in graphite electrode. The schematic illustration of three-electrode device is shown in **Figure S11**, which consists of graphite (working electrode), lithium string (reference electrode), lithium foil (counter electrode) and two pieces of separators. The electrochemical impedance spectra (EIS) measurements (**Figure 3a and 3b)** under various temperatures were tested and corresponding activation energies (E_a) were calculated based on Arrhenius equation (**Figure 3c and 3d**).[22] The charge-transfer resistance (R_{ct}) and interfacial resistance (R_{SEI}) derived E_a values are 45.7 and 24.6 kJ mol^{-1} respectively for G@TC electrode, similar to those on G electrode (45.3 and 22.0 kJ mol^{-1}). This indicates that both the energy barriers in passing through the SEI layer and striping solvation sheath are comparable for G and G@TC electrodes. This result is consistent with the similar SEI ingredients between G and G@TC electrodes **(Figure S9)**. Worth noting that, when comparing the absolute values of these individual resistance recorded, it can be observed that the dynamic behavior of Li^+ in G@TC is evidently faster than that of G electrode (**Figure 3a and 3b**), deducing that the pre-exponential factor of G@TC is higher than that of G according to Arrhenius equation. The larger pre-exponential factor is ascribed to more active sites in G@TC anode.[23] The high anisotropy of graphite allows Li^+ to intercalate only through its edge-plane rather than basal-plane.[24] After coating an amorphous carbon layer on graphite sheets, the active sites at edge side of

graphite bulk become less. Therefore, it is reasonable to infer that the more active sites should be ascribed to the contribution from basal-plane side.

The EIS at room temperature were further associated (**Figure S12**). The G@TC electrode exhibits higher bulk resistance (R_e) due to the introduction of amorphous carbon, while smaller R_{SEI} and R_{ct} at high frequency and medium frequency of EIS spectra are observed on G@TC anode. This confirms faster charge transfer process. The Warburg coefficient (σ) was compared and the G@TC electrode exhibits lower σ value (**Figure 3e**).[25] The R_{ct} derived exchange current density (j_0) can be calculated according to the following equation:[26]

$$j_0 = \frac{RT}{nFR_{ct}A} \quad (1)$$

where R is the gas constant, T is the absolute temperature, n is the number of electrons per molecule during redox reaction, A is the area of the electrode/electrolyte interface. The larger j_0 value indicates more favorable lithiation of G@TC electrode (**Figure 3f**). Consequently, more active sites at basal-plane are favorable for improving ionic diffusion and facilitating Li^+ intercalation in bulk graphite.

The galvanostatic intermittent titration technique (GITT) measurements of G and G@TC half-cell were collected from three-electrode batteries (**Figure 4a**). This can probe the actual polarization and Li^+ diffusion coefficient of graphite material and exclude the influence of Li counter electrode. The lower voltage hystersis and ohmic polarization can be effectively achieved for G@TC than G electrode especially at high lithiation degree (**Figure 4c**), ascribing to more active sites and the improved ionic diffusion pathways. Moreover, lithium ion diffusions within both G and G@TC are assumed to obey the Fick's second law of diffusion, and the lithium ion diffusion coefficient (D_{Li^+}) can be calculated according to the following equation:[27]

$$D_{Li^+} = \frac{4}{\tau\pi}\left(\frac{m_B V_M}{M_B S}\right)^2 \left(\frac{\Delta E_S}{\Delta E_\tau}\right)^2 \quad (2)$$

where τ is the constant current discharging time; m_B, V_M, and M_B are the mass, molar volume, and molar mass of the active material, respectively; ΔE_S and $\Delta E\tau$ are the change of the steady state voltage and the total change of cell voltage during the constant current discharging, respectively, which can be obtained from **Figure 4b**. The calculated D_{Li^+} from GITT are 6.6×10^{-10} and 0.7×10^{-10} cm^2 s^{-1} at x=0.4 and 0.7 in Li_xC_6 respectively for G@TC (**Figure 4d**), which are both higher than that of G electrode (3.5×10^{-10} and 0.4×10^{-10} cm^2 s^{-1}), consistent with the trends of σ illustrated in **Figure 3e** and previous publication.[28] Furthermore, the charge-discharge curves of G and G@TC electrodes at different current densities are compared (**Figure S13**). A lower polarization is detected on G@TC anode. This difference becomes more pronounced at higher current density, demonstrating the superior rate performance of turbostratic carbon coated graphite (**Figure 2**).

Generally, the diffusion rate of Li^+ at basal-plane of graphite sheets is much lower than that at edge-plane, leading to the preferential Li^+ intercalation from the edge of graphite layers (**Figure 5a**), which is unfavorable for lithiation of Li_xC_6 when x approaches 1 and especially untoward at high current densities. After coating graphite sheets with nanoscale turbostratic carbon layer (**Figure 5b**), except for the entrance of Li^+ at the edge side, G@TC can also afford active sites for Li^+ at the basal-plane. The larger interlamellar spacing and amorphous nature of coated turbostratic carbon layer removes the anisotropy of graphite surface and enables rapid delivery of Li^+ to the edge of graphite where it can insert, resulting in increased Li^+ diffusion rate and decreased polarization.[29] Therefore, the coating of graphite with turbostratic carbon layer benefits the high-rate electrochemical performance in LIBs.

3. Conclusions

In summary, graphite anode with high rate performance was achieved by coating nanoscale turbostratic carbon layer on surface. Compared with raw graphite flakes, additional active sites and Li^+ diffusion layer from the basal-plane of graphite sheets were provided by a thin turbostratic

carbon coating. Li^+ transport is largely facilitated due to its isotropy and larger interlamellar spacing. Consequently, G@TC exhibits a decreased polarization and increased Li^+ diffusion coefficient. This work deeply enriches the knowledge of improving the rate performance of graphite anode through nanoscale interfacial coating, accelerating the practical fast-charging applications of graphite anode without lithium plating.

Supporting Information

Supporting Information is available from the Wiley Online Library or from the author.

Acknowledgements

W.-L.C. and Y.C. contribute equally. This work was supported by National Natural Science Foundation of China (21776019, 21825501, and U1801257), National Key Research and Development Program (2016YFA0202500 and 2016YFA0200102), the Tsinghua University Initiative Scientific Research Program, Department of Science and Technology of Jilin Province (20180520014JH), Education Department of Jilin Province (JJKH20180549KJ), and Science and Technology Innovative Development Program of Jilin City (201831737). W. L. Cai appreciates the Shuimu Tsinghua Scholar Program of Tsinghua University.

Conflict of Interest

The authors declare no conflict of interest.

Received: ((will be filled in by the editorial staff))
Revised: ((will be filled in by the editorial staff))
Published online: ((will be filled in by the editorial staff))

References

[1] F. Ding, W. Xu, D. Choi, W. Wang, X. Li, M. H. Engelhard, X. Chen, Z. Yang, J.-G. Zhang, *J. Mater. Chem.* **2012**, *22*, 12745; X. G. Yang, G. Zhang, S. Ge, C. Y. Wang, *Proc. Natl. Acad. Sci. U. S. A.* **2018**, *115*, 7266-7271; X. Cao, Y. Xu, L. Zhang, M. H. Engelhard, L. Zhong, X. Ren, H. Jia, B. Liu, C. Niu, B. E. Matthews, H. Wu, B. W. Arey, C. Wang, J.-G. Zhang, W. Xu, *ACS Energy Lett.* **2019**, *4*, 2529-2534; X. Q. Zhang, T. Li, B. Q. Li, R. Zhang, P. Shi, C. Yan, J. Q. Huang, Q. Zhang, *Angew. Chem. Int. Ed.* **2020**, *59*, 2-8; J.-X. Chen, X.-Q. Zhang, B.-Q. Li, X.-M. Wang, P. Shi, W. Zhu, A. Chen, Z. Jin, R. Xiang, J.-Q. Huang, Q. Zhang, *J. Energy Chem.* **2020**, *47*, 128-131.

[2] X.-G. Yang, T. Liu, Y. Gao, S. Ge, Y. Leng, D. Wang, C.-Y. Wang, *Joule* **2019**, *3*, 3002-3019.

[3] F. S. Li, Y. S. Wu, J. Chou, N. L. Wu, *Chem. Commun.* **2015**, *51*, 8429-8431; M. Lu, Y. Tian, X. Zheng, J. Gao, B. Huang, *J. Power Sources* **2012**, *219*, 188-192; C. Yan, Y.-X. Yao, W.-L. Cai, L. Xu, S. Kaskel, H. S. Park, J.-Q. Huang, *J. Energy Chem.* **2020**, *49*, 335-338.

[4] N. Kim, S. Chae, J. Ma, M. Ko, J. Cho, *Nat. Commun.* **2017**, *8*, 812.

[5] Q. Liu, C. Du, B. Shen, P. Zuo, X. Cheng, Y. Ma, G. Yin, Y. Gao, *RSC Adv.* **2016**, *6*, 88683-88700.

[6] H. Lu, X. Chen, Y. Jia, H. Chen, Y. Wang, X. Ai, H. Yang, Y. Cao, *Nano Energy* **2019**, *64*, 103903.

[7] W. Qi, L. Ben, H. Yu, Y. Zhan, W. Zhao, X. Huang, *J. Power Sources* **2019**, *424*, 150-157; L. Zhang, L. Chai, L. Zhang, M. Shen, X. Zhang, V. S. Battaglia, T. Stephenson, H. Zheng, *Electrochim. Acta* **2014**, *127*, 39-44; J. Qian, W. A. Henderson, W. Xu, P. Bhattacharya, M. Engelhard, O. Borodin, J. G. Zhang, *Nat. Commun.* **2015**, *6*, 6362; Q. Q. Liu, L. Ma, C. Y. Du, J. R. Dahn, *Electrochim. Acta* **2018**, *263*, 237-248; G. L. Zhu, C. Z. Zhao, J. Q. Huang, C. He, J. Zhang, S. Chen, L. Xu, H. Yuan, Q. Zhang, *Small* **2019**, *15*, e1805389.

[8] Y. Yamada, K. Furukawa, K. Sodeyama, K. Kikuchi, M. Yaegashi, Y. Tateyama, A. Yamada, *J. Am. Chem. Soc.* **2014**, *136*, 5039-5046.

[9] D. S. Kim, Y. E. Kim, H. Kim, *J. Power Sources* **2019**, *422*, 18-24.

[10] J.-H. Shim, S. Lee, *J. Power Sources* **2016**, *324*, 475-483; Q. Cheng, R. Yuge, K. Nakahara, N. Tamura, S. Miyamoto, *J. Power Sources* **2015**, *284*, 258-263.

[11] J. Luo, C.-E. Wu, L.-Y. Su, S.-S. Huang, C.-C. Fang, Y.-S. Wu, J. Chou, N.-L. Wu, *J. Power Sources* **2018**, *406*, 63-69; F. S. Li, Y. S. Wu, J. Chou, M. Winter, N. L. Wu, *Adv. Mater.* **2015**, *27*, 130-137.

[12] J. Gao, L. J. Fu, H. P. Zhang, L. C. Yang, Y. P. Wu, *Electrochim. Acta* **2008**, *53*, 2376-2379; H. Li, H. Zhou, *Chem. Commun.* **2012**, *48*, 1201-1217; H. Zeng, J. He, D. Fang, Y. Liang, R. Zhao, Y. Cai, D. Lu, *Energy Technol.* **2019**, 1801078.

[13] C. Yan, R. Xu, J. L. Qin, H. Yuan, Y. Xiao, L. Xu, J. Q. Huang, *Angew. Chem. Int. Ed.* **2019**, *58*, 15235-15238.

[14] A. Carrillo, J. A. Swartz, J. M. Gamba, R. S. Kane, N. Chakrapani, B. Wei, P. M. Ajayan, *Nano Lett.* **2003**, *3*, 1437-1440.

[15] Y.-J. Han, J. Kim, J.-S. Yeo, J. C. An, I.-P. Hong, K. Nakabayashi, J. Miyawaki, J.-D. Jung, S.-H. Yoon, *Carbon* **2015**, *94*, 432-438; C. Wan, H. Li, M. Wu, C. Zhao, *J. Appl. Electrochem.* **2009**, *39*, 1081-1086; M. Yoshio, H. Wang, K. Fukuda, T. Umeno, T. Abe, Z. Ogumi, *J. Mater. Chem.* **2004**, *14*, 1754-1758.

[16] R. Xu, C. Yan, Y. Xiao, M. Zhao, H. Yuan, J.-Q. Huang, *Energy Storage Mater.* **2019**, 10.1016/j.ensm.2019.1012.1020.

[17] J.-L. Shi, C. Tang, J.-Q. Huang, W. Zhu, Q. Zhang, *J. Energy Chem.* **2018**, *27*, 167-175.

[18] S. Yoon, H. Kim, S. M. Oh, *J. Power Sources* **2001**, *94*, 68-73.

[19] C. Birkenmaier, B. Bitzer, M. Harzheim, A. Hintennach, T. Schleid, *J. Electrochem. Soc.* **2015**, *162*, A2646-A2650; P. Arora, M. Doyle, R. E. White, *J. Electrochem. Soc.* **1999**, *146*, 3543-3553.

[20] T. Zhu, Q. Hu, G. Yan, J. Wang, Z. Wang, H. Guo, X. Li, W. Peng, *Energy Technol.* **2019**, *7*, 1900273.

[21] J. Hou, M. Yang, D. Wang, J. Zhang, *Adv. Energy Mater.* **2020**, 1904152.

[22] K. Xu, Y. Lam, S. S. Zhang, T. R. Jow, T. B. Curtis, *J. Phys. Chem. C* **2007**, *111*, 7411-7421.

[23] X. Xie, Y. Li, Z. Q. Liu, M. Haruta, W. Shen, *Nature* **2009**, *458*, 746-749.

[24] K. Persson, V. A. Sethuraman, L. J. Hardwick, Y. Hinuma, Y. S. Meng, A. van der Ven, G. Ceder, *J. Phys. Chem. Lett.* **2010**, *1*, 1176-1180; Z. Ma, Y. Zhuang, Y. Deng, X. Song, X. Zuo, X. Xiao, J. Nan, *J. Power Sources* **2018**, *376*, 91-99.

[25] T. Xu, N. Lin, W. Cai, Z. Yi, J. Zhou, Y. Han, Y. Zhu, Y.Qian, *Inorg. Chem. Front.* **2018**, *5*, 1463-1469.

[26] L. Wang, J. Zhao, X. He, J. Gao, J. Li, C. Wan, C. Jiang, *Int. J. Electrochem. Sci.* **2012**, *7*, 345-353.

[27] H. Zhou, F. Xin, B. Pei, M. S. Whittingham, *ACS Energy Lett.* **2019**, *4*, 1902-1906.

[28] P. Yu, B. N. Popov, J. A. Ritter, R. E. White, *J. Electrochem. Soc.* **1999**, *146*, 8-14.

[29] B. Kang, G. Ceder, *Nature* **2009**, *458*, 190-193.

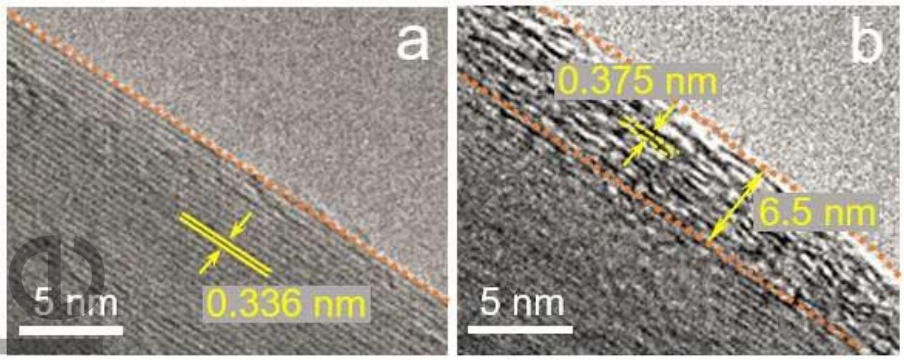

Figure 1. The morphology of the pristine and nanoscale turbostratic carbon coated graphite. TEM images of (a) G and (b) G@TC.

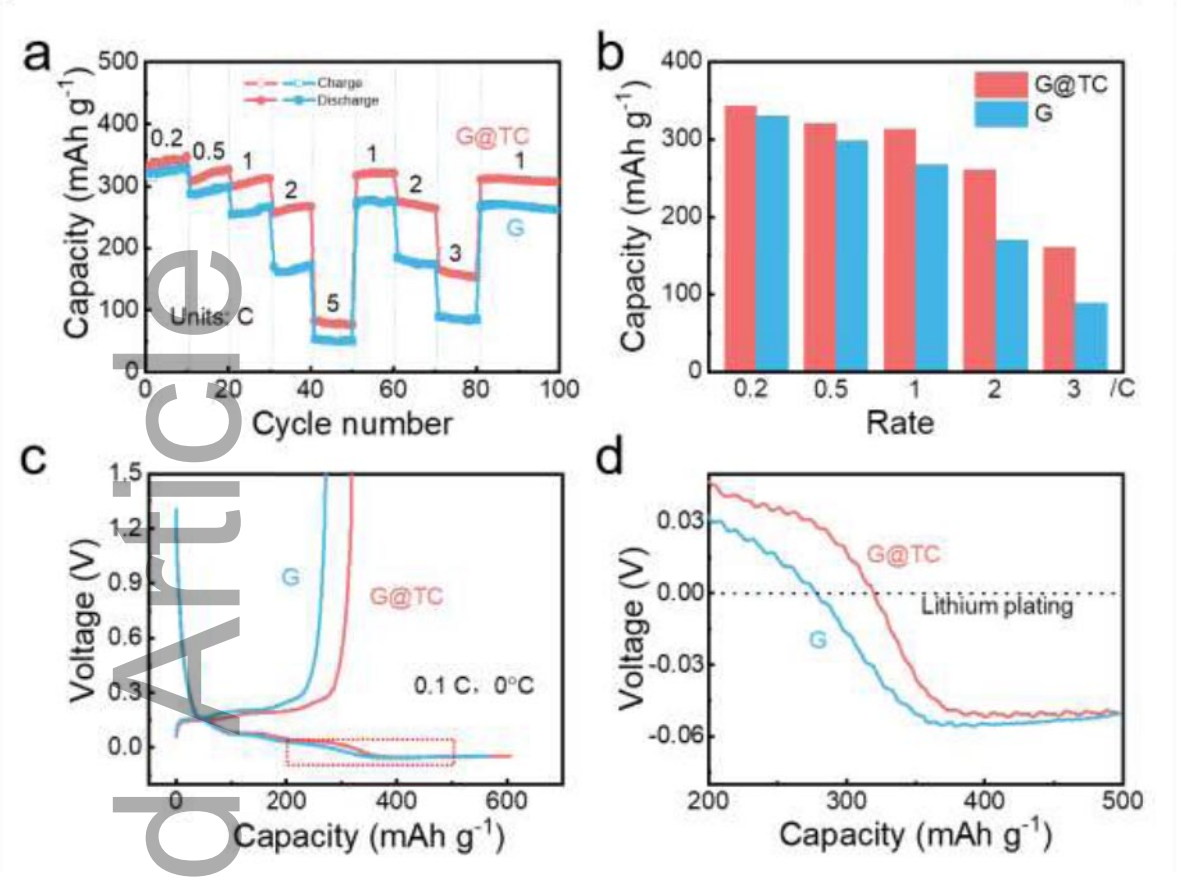

Figure 2. Electrochemical performance of G and G@TC half-cell using conventional two-electrode batteries. (a) Rate capabilities at different current densities of G and G@TC electrodes under room temperature and (b) corresponding bar chart, (c, d) charge-discharge curves of G and G@TC electrodes at rate of 0.1 C under 0°C .

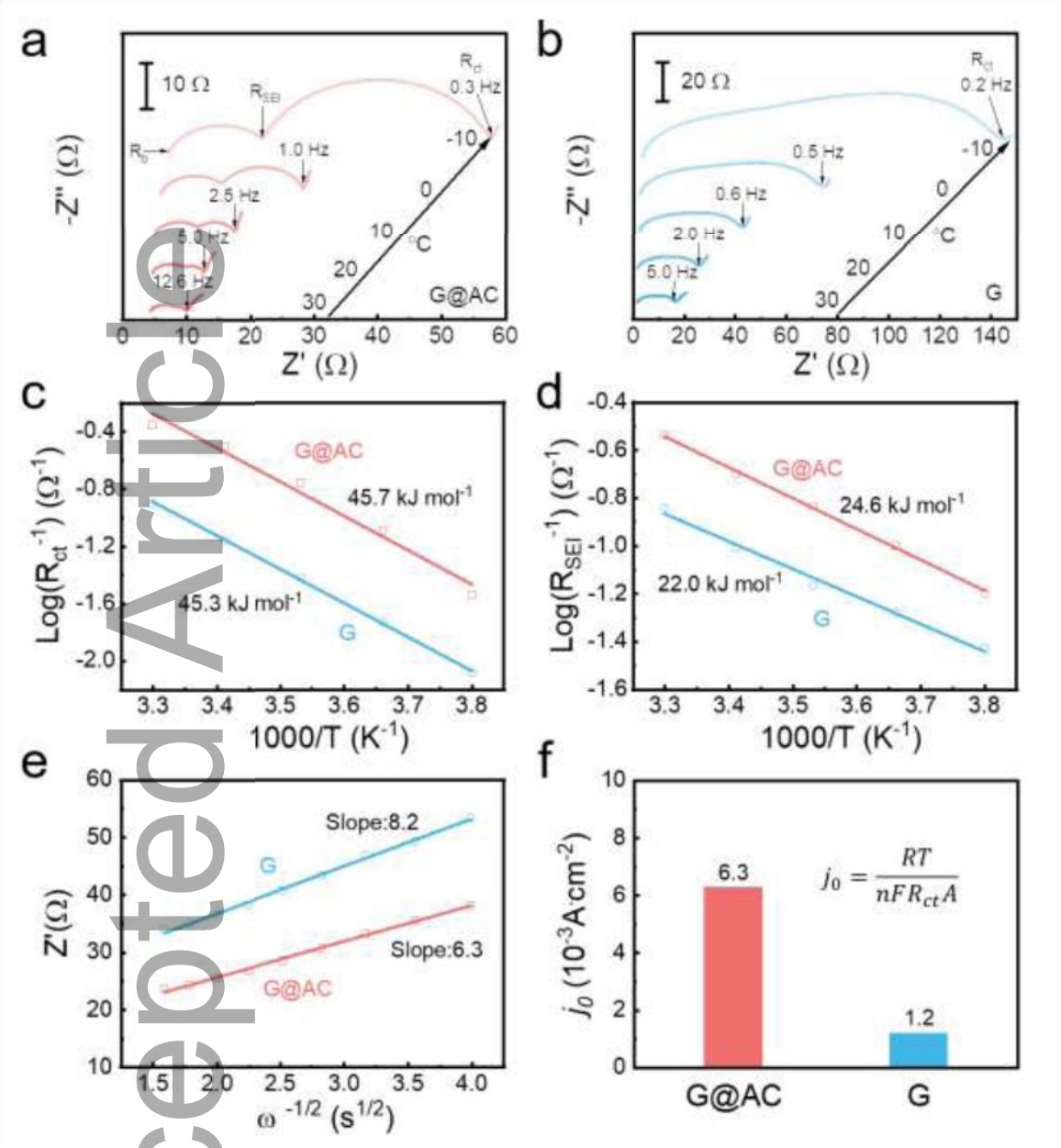

Figure 3. The electrochemical impedance spectra at different temperature of (a) G@TC and (b) G electrodes, and corresponding (c) charge-transfer impedance derived activation energies and (d) graphite/electrolyte interphases impedance derived activation energies; (e) Warburg coefficient plots and the (f) exchange current densities of G and G@TC electrodes at room temperature.

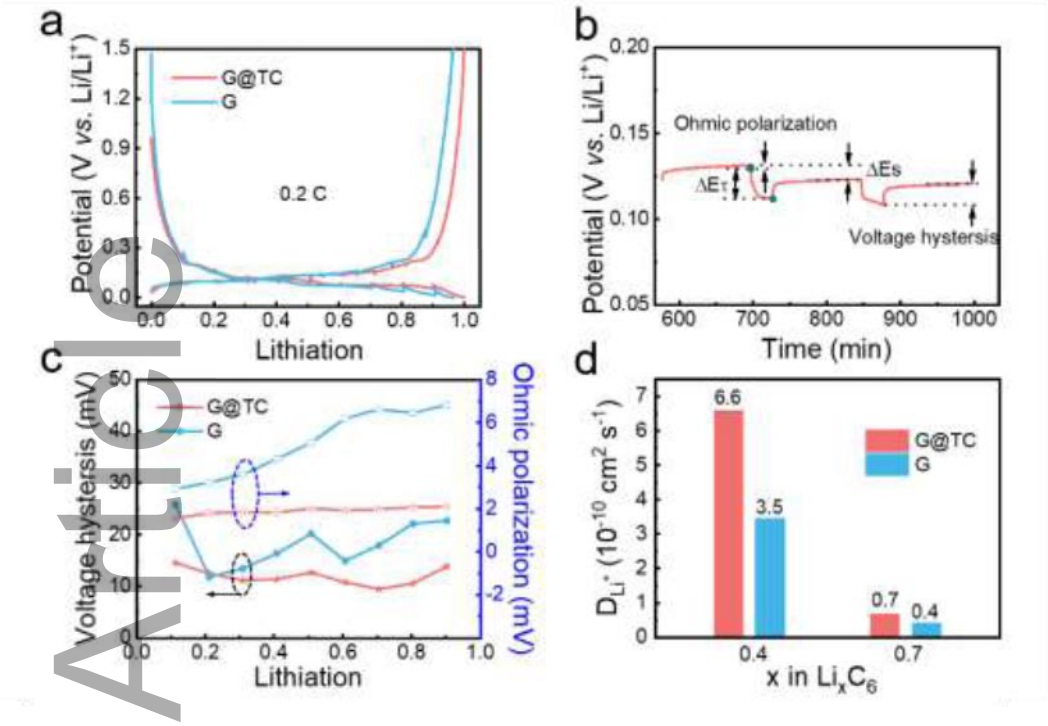

Figure 4. The GITT measurements of G and G@TC half-cell based on three-electrode battery. (a) The voltage profiles *vs.* degree of lithiation of GITT measurements at the rate of 0.2 C, (b) the zoomed-in voltage *vs.* time curve from the GITT measurement, derived (c) voltage hystersis and ohmic polarization, and (d) lithium ion diffusion coefficients of G and G@TC electrodes.

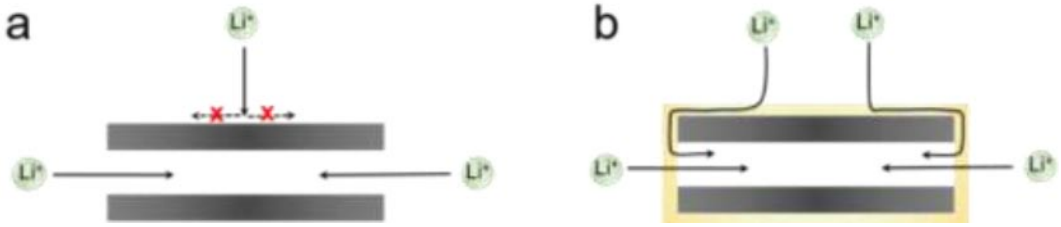

Figure 5. Scheme of the lithium ion diffusion into graphite anode. (a) The lithium ion diffusion into G from only edge side is slow and (b) G@TC can provide additional entrance at the basal-plane by coated turbostratic carbon layer, benefiting for fast lithium ion diffusion into G@TC.

Keywords: fast-charging electrode

*Wenlong Cai, Chong Yan, Yu-Xing Yao, Lei Xu, Rui Xu, Li-Li Jiang, Jia-Qi Huang, and Qiang Zhang**

Rapid Lithium Diffusion in Order@Disorder Pathways for Fast-Charging Graphite Anodes

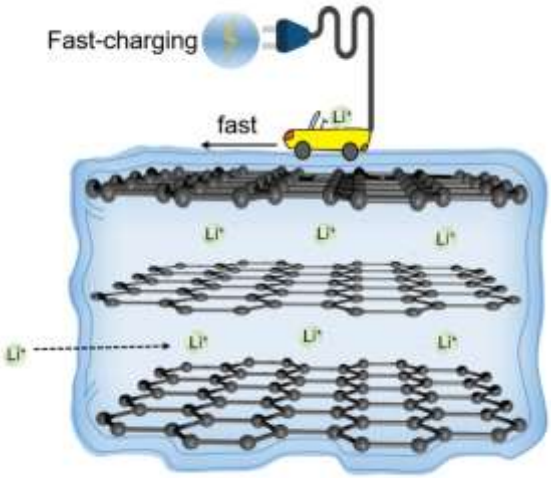

The turbostratic carbon layer on graphite anode affords abundant active sites and fast diffusion pathways to accelerate the transportation of Li ions in a working battery. This renders a reduced polarization and significantly improved rate performance.